ESTIMATING ERROR BOUNDS OF QUANTITATIVE SCHLIEREN IMAGING FOR TURBOMACHINERY APPLICATIONS

Tsinoglou, M.
Kalfas, A.
Aristotle University of Thessaloniki, Laboratory of Fluid Mechanics and Turbomachinery, Department of Mechanical Engineering, GR-54124, Thessaloniki, Greece

Terzis, A.
Technion - Israel Institute of Technology, Thermo-Fluids and Interfaces Laboratory, Department of Aerospace Engineering, IL- 3200003, Haifa, Israel

Mitra, A.
Cukurel, B.
Technion - Israel Institute of Technology, Turbomachinery and Heat Transfer Laboratory, Department of Aerospace Engineering, IL- 3200003, Haifa, Israel

ABSTRACT

Flow observation measurements via optical systems can have significant amount of uncertainty due to light intensity fluctuations. The present work introduces a novel method of identifying uncertainty bounds in schlieren measurements. The objective is to identify uncertainty caused by vibrations of the optical component of schlieren, in micro gas turbine blade testing.

The calculation process of uncertainty is based on the image intensity fluctuation caused by knife's edge vibrations. Application of the method in horizontal and vertical knife's edge orientations aided in defining the vibrations in two axes. The flexural rigidity of the optical system was increased, from 6.05 to 291.7 $Pa \times m^4$ *in the main axis, and the two orientations were tested again. The overall uncertainty decreased once the rigidity was increased, demonstrating that the optical system's deformation vibrations are the cause of intensity fuctuation. An overall decrease in maximum density gradient deviation of 9.39% and 14.01% for horizontal and vertical cutoff respectively was observed. The fluctuation results matched the intensity of the corresponding frames, validating the precision of the method. A dominant frequency was revealed for each case and a common behavior of all cases in high frequency and low amplitude was resolved. It became evident that the method's capacity to determine uncertainty is sufficient for a wide range of frequency and amplitude vibrations.*

The significance of this method is attributed to the measurement of vibrations without any additional instrumentation. The measurement is made exclusively by the optical system and is flexible in use for most schlieren systems.

NOMENCLATURE

c	Speed of light
f	Focal length of calibration lens
i	Iteration number
k	Gladstone-Dale coefficient
n	Refractive index
r	Radius of calibration lens
L	Phenomenon thickness

Subscripts

in	Inlet condition
tot	Total quantity
0	Quantity in ambient conditions

Greek characters

ε	Refraction angle
ρ	Density

Abbreviations

AOI	Area Of Interest
BIA	Bottom Isolated Area
CO%	Percentage of Cut-Off
DL	Digital Level
RMSe	Root Square Mean error
PR	Pressure ratio
TLC	Transonic Linear Cascade

INTRODUCTION

In scope of identifying the aerodynamic performance of micro gas turbine blades a schlieren system was built around the Transonic Linear Cascade (TLC) of Turbomachinery and Heat Transfer Laboratory at Technion Israel Institute of Technology. The cascade is designed for experiments on micro gas turbine blades with many varying parameters such as inlet Mach number, Reynolds number, inlet pressure, inlet temperature, stagger and incidence angle as described in detail by Yakirevich et al [1]. In order to observe the local density gradients, a schlieren imaging system is used to visualize the compressible flow in the cascade. Early Schlieren measurements of Dunsby [2], followed by studies of Zhou et al [3], Loose et al [4], Leonard et al [5] and Passman et al [6], to name a few, shows the popularity of the technique. Quantification of schlieren measurements introduced later mainly with the three primary calibration methods of Hagareth et al [7].

In schlieren imaging measurements a uniform background of constant intensity should be maintained throughout the recording process. Toepler's schlieren method is based on the cutoff of many elementary images with the knife's edge cutoff creating a uniform darkening if placed precisely at the focal point. The background intensity is varied by changing the position of the knife's edge, i.e., changing the percentage of light cutoff (CO%) at the focal point (Figure 1). As a result, the calibration curve used for the quantification of the schlieren will vary accordingly to the variation of the relative position of the knife's edge. Ideally, if the schlieren system is presumed to be a rigid body, relative position of the knife's edge with respect to the light source and the camera would not change. Hence, in this case there should be no fluctuations of background intensity. However, in reality each optical component vibrates with its own characteristic vibration constants, giving rise to background intensity fluctuations.

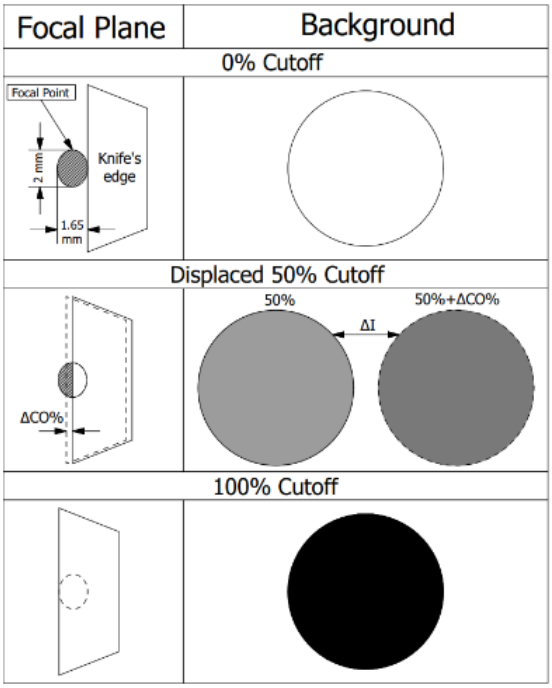

Figure 1. Background intensity variation with respect to percentage of cutoff

Vibrations in wind tunnel experiment can corrupt optical results and introduce significant uncertainty in measurements. Troublesome vibrations in high speed and high vorticity tests corrupting schlieren results have been noted by Venkatakrishnan [8] et al and Adam et al [9]. Wells [10] devised a controller to actively counteract the knife's edge movement in order to minimize the error sourcing from vibrations. Since vibrations are so erroneous a method to assess the introduced uncertainty is a valuable tool.

In order to quantify the level of vibration, a method based on intensity variation was created. A similar procedure of background intensity mapping with respect to knife's edge position was followed by Alveraz-Herrera et al [11] with a view to achieve an alternative method of calibration. The uncertainty of the measurement is attributed to the intensity fluctuation and the quantification method resulting in density gradient deviation. The outcome is an indication of the stability and therefore the precision of the density gradient acquired by the schlieren. In what follows, the paper describes the methodology of uncertainty quantification in detail, thereafter, applying the same to some test cases at transonic speeds, and subsequently discusses the results and implications.

METHODS

1. Theory of calibrated schlieren

Gladstone and Dale [12] relation for refractive index (n) and density of the media (ρ) is :

$$n = \frac{c_0}{c} \geq 1, \quad n = k\rho + 1 \qquad (1)$$

In this study the medium under observation is air, thus the value of c in equation 1 represents the local light speed through the air in the cascade. The Gladstone-Dale coefficient is assumed to be constant and equal to $2.23 \times 10^{-4}\ [m^3/kg]$. The flow is not externally heated or cooled. The operating principle of schlieren is that the bending of light is caused by the integrated gradient of the refractive index in the medium Settles [13] and Arts [14]. In this work the schlieren governing equations comply with Kook et al [15]. The working equation is equation 2 describing the deflection to the gradient of refractive index which is obtained by differentiating equation 1.

$$\varepsilon_y = \frac{L}{n_0}\frac{\partial n}{\partial y} = \frac{kL}{n_0}\frac{\partial \rho}{\partial y}, \varepsilon_x = \frac{L}{n_0}\frac{\partial n}{\partial x} = \frac{kL}{n_0}\frac{\partial \rho}{\partial x} \qquad (2)$$

In order to obtain a quantitative information from the Schlieren images, one needs a mapping of pixel intensity to light deflection (or the density gradient by equation 2). This calibration process is a paramount step in the calibrated schlieren technique (Hagareth et al [7]). For calibration, an extremely weak plano-convex lens (of 1" diameter and 10m focal length) is used. The calibration lens was chosen such that the density gradients range comply with the gradient range of the transonic flow calculated based on the findings of Kojima et al [16]. The calibration lens is placed as illustrated in figure 2a. The image of the calibration lens has a monotonic variation of intensity from bright to dark as one moves the vertical knife's edge from right to left. The light refraction caused by the lens can be calculated from the expression below.

$$\tan(\varepsilon) \approx \varepsilon = \frac{r}{f} \qquad (3)$$

Due of axisymmetry of the lens , equation 3 is valid for both x and y direction refractions.

Combination of equations 2 and 3 form a relation of density gradients as a function of the lens' radius.

$$\frac{\partial \rho}{\partial r} = \frac{n_0\, r}{k\, L\, f} \qquad (4)$$

The calibration curve is obtained through the intensity distribution in the image of the calibration lens and the theoretical refractive index gradient distribution on the calibration lens radius (r).

2. Calibration map

The knife's edge is posted on micrometers that can be move accurately in x-y-z direction. It is possible to identify the size of the focal point by traversing the knife's edge from complete darkening to saturation. The amount of distance traveled by the blade from darkening to saturation is equal to the size of the focal point in the respective direction. The dimensions of the focal point were found to be 1.65 and 2 mm in the horizontal and vertical direction respectively. The correlation between percentage of cutoff and the intensity distribution on the lens was achieved with a 10% step change in cutoff (0.165 mm horizontally and 0.2 mm and vertically).

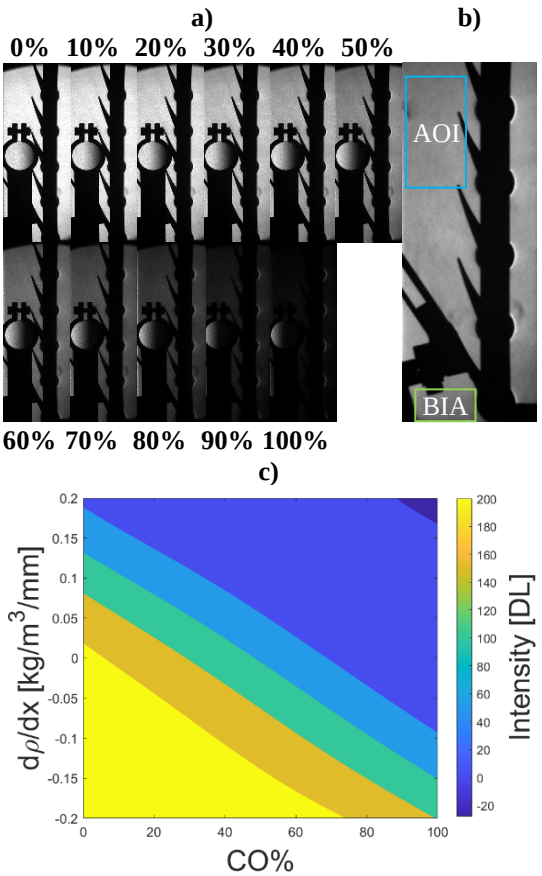

Figure 2. Calibration with varying cutoff b) Presentation of Area of interest and Bottom Isolated Area c) Calibration map

In the present uncertainty estimation, the calibration process is repeated for each position of the knife's edge – i.e., from 0% to 100% CO. The calibration image of each step for vertical cutoff is presented in Figure 2a. Eleven calibration curves of are obtained and two interpolation polynomials of degree 5 are employed to generate a calibration surface. A planar slice of this surface at some %CO represent the calibration curve relating the pixel intensity to density gradient. Such calibration surfaces were obtained for each of the four experimental cases in table 1.

The obtained calibration map is used to calculate the uncertainty based on the light intensity calculations thoroughly explained in the following chapters. In order to accurately quantify the uncertainty a reference with known conditions needs to be acquired.

3. Reference

The intensity fluctuation was measured with respect to a known reference intensity. The average intensity of 100 images before the start of the phenomenon for each case, is taken as the reference intensity. It is a priori known that the intensity level in (AOI), before the start of the experiment, corresponds to 50% CO. The density gradient of the background should be zero, but a small deviation is always present. The density gradient of the background is calculated from the 50% CO% calibration curve for the reference intensity.

4. Uncertainty calculation

The area of interest (AOI) is located at the downstream of the blades where the shockwave patterns appear. The AOI region, shown as a blue rectangle in figure 2b, is a region of active flow which will inherently have intensity fluctuation due to the flow. It is impossible to decompose the intensity fluctuations in this region due to the actual flow and the vibration of the system. However, the bottom isolated area (BIA), marked in green in figure 2b, is a region of no flow below the guiding tailboards.

The background intensity in BIA is relatively uniform, but it does not match exactly that of AOI due to optical aberrations. Notwithstanding, their intensity ratio (IR) was relatively uniform over the full range of %CO. The ratio was obtained from equation 5 as the mean of the intensities in the AOI and BIA for 100 reference frames. From this procedure a correlation of IR to CO% is extracted.

$$IR_i = \frac{mean(I_{AOI})_{xyt,i}}{mean(I_{BIA})_{xyt,i}}, \qquad i = 0\%, 10\% \ldots 100\% \qquad (5)$$

The intensity fluctuation calculations are applied iteratively for each frame. The Intensity ratio (IR) is obtained by the IR vs CO curve for the percentage of cutoff of the previous frame, since the percentage of cutoff of the current frame is yet to be found. The mean intensity of AOI is calculated from the IR value and the mean intensity of BIA (equation 6).

$$I_{AOI,i} = I_{BIA,i} \times IR_i(CO_{i-1}) \quad (6)$$

The actual instantaneous CO% for each frame can be found from the calibration map (figure 2c). The percentage of cutoff is found based on the calculated intensity for the ambient density gradient. A planar slice of the 3d curve represented as map in figure 2c in the known ambient density gradient gives the CO% to Intensity correlation curve of figure 3.

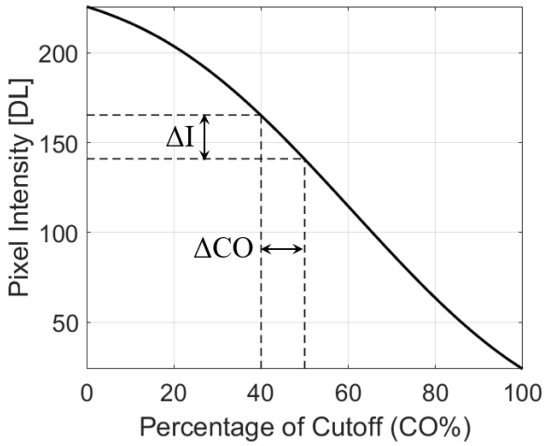

Figure 3. Background Intensity as a function of CO% for reference ambient density gradient

Returning to the calibration map, with 50% cutoff and the respective intensity, the uncorrected density gradient is calculated. The density gradient deviation can be expressed as the difference of density gradients of actual and 50% CO% calibration curve.

$$\left(\frac{\partial \rho}{\partial x}\right)_{Error} = \frac{\partial \rho}{\partial x}_{CO=CO(I_{bg})} - \frac{\partial \rho}{\partial x}_{CO=50\%} \quad (7)$$

Equation 7 expresses the density gradient deviation calculated in the vibration identification method. A flowchart that summarizes the calculation process in detail is presented by Tsinoglou [17].

The error of this method is attributed to the inability of the surface fitting to completely match the values of the actual calibration curves. The maximum local error of the surface appeares near the dynamic range limits and was found to be 3.75%. The mean error is calculated as the average calibration curve-fitted surface mismatch of all points. A mean error of 0.8% indicated the accuracy of the method. In order to make the identification method more accurate, one can use a better fitted surface by optimizing the grade of polynomial in the two directions.

EXPERIMENTAL SETUP

Z-type schlieren is setup in the present investigation. This setup is relatively simple to set with low aberrations and sufficient sensitivity (Settles [13]). The sensitivity of a schlieren system is increased as the focal length of the mirrors increases (Settles [13], Davies [18], Pavlov et al [19]) and the larger the diameter the larger the field of view. For the specific schlieren system two 8-inch (0.2032 m) diameter parabolic mirrors with focal length of f/5 = 40 inches (1.016 m) were employed. Optical equipment of this type is relatively heavy. Since the light source should be placed at the focal length of the first parabolic mirror the parabolic mirrors should have been place roughly 1-1.5 meters far from the cascade. Such distance would create huge vibrations by the exitance of the heave parabolic mirrors. For this reason, a double folded schlieren system was chosen to bring the parabolic mirrors closer to the cascade which is the source of the exitance. The double folding was achieved with the use of two 100x100 mm plane mirrors that redirect the light beam in the opposite direction. The complete experimental setup is presented in figure 4.

The schlieren system was chosen to be mounted on the cascade to maintain the optical path in case of the cascade's movement. A combination of dampening optical tables and air dampeners was used to isolate the optical system of the TLC forces. An aluminum breadboard is mounted to air dampeners. The aluminum breadboard extends to the sides of the cascade and supports 2 identical thick optical tables on which the optical components are mounted. The forces applied to the cascade by the supersonic flow have to pass through the air dampeners in order to get transmitted to the optical system. The thin aluminum breadboard was deformed due to the load of the optical components and tables thus creating deformative vibrations. The deformation of the breadboard was observed to be mostly in Y axis with the elastic line having the shape noted in figure 4. To increase the aluminum breadboard's rigidity 4 aluminum bars with orthogonal cross section and dimensions of 80x40x620 mm where used. The bars were placed with the 80 mm side perpendicularly to the breadboard to achieve the maximum increase in flexural rigidity.

For the schlieren recording an IDT motion pro Y7-S1 high speed camera with frame rate of 5300 fps and exposure time of 1 μs was used. A total amount of 10000 frames that correspond to 1.8868 s of filming time was selected and analyzed. The starting and ending frames were selected such that the whole vibrating phenomenon is included to the analysis.

TEST CASES

The method was tested for 4 cases. Two orientations were tested before and after the increase of schlieren system's flexural rigidity. The flexural rigidity in the main axis was increased from 6.05 to 291.7 $Pa * m^4$ by additional supporting structure.

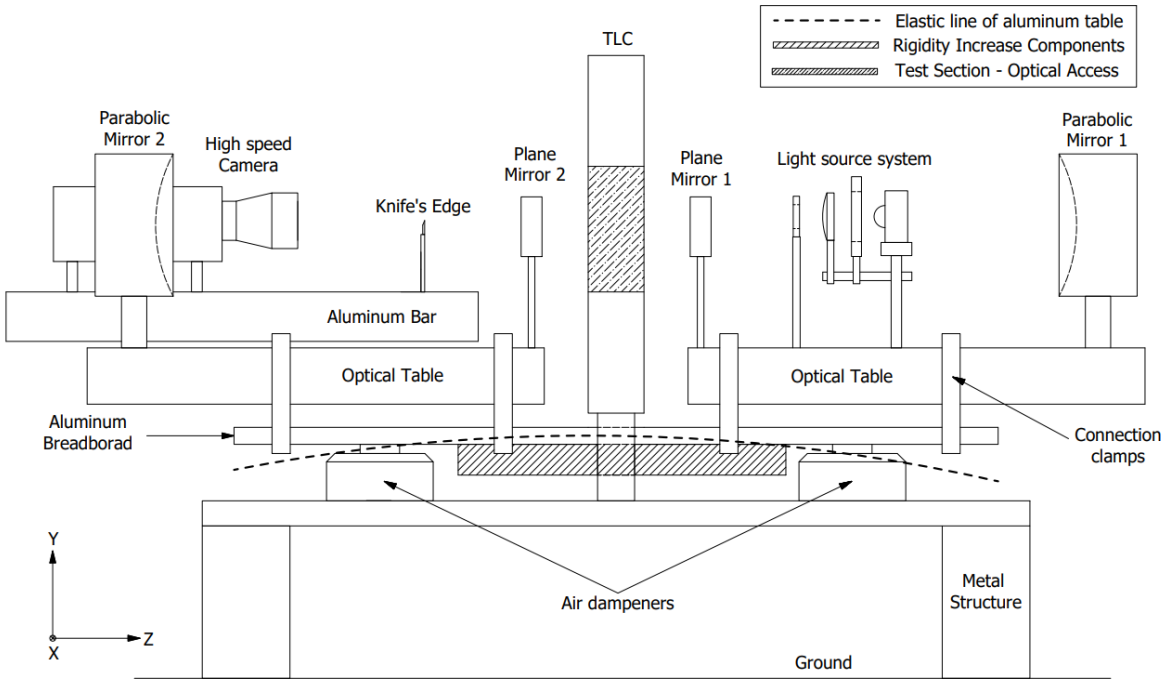

Figure 4. Schematic of experimental setup

Vibrations in X-Y axes are observed by placing the knife's edge in vertical (Y) and horizontal (X) orientation respectively.

It is assumed that the vibrations in Z axis are negligible and do not introduce light intensity variation comparable to X and Y axis vibrations. Exciting the system only in Z direction through external force did not show any light fluctuation in comparison to the other two axes, confirming that the contribution of Z axis to the vibrations where negligible.

Table 1. Test case conditions

Case	Cutoff	Rigidity	PR	$T_{tot,in}$ [K]
H1	Horizontal	Normal	3	296
V1	Vertical	Increased	3	296
H2	Horizontal	Normal	3	296
V2	Vertical	Increased	3	296

All four cases were tested for the same pressure ratio that resulted in transonic flow. The inlet conditions were kept identical with inlet total temperature of 296 K and inlet total pressure of 3 bars as the flow was expanded in atmospheric conditions. The conditions of each case are summarized in table 1. By keeping identical conditions, the results can be compared and validated.

The Tests were performed for a set of 7 NASA C3X guide vanes. The geometrical characteristic of the vanes are based in Hylton's work [20] with the detailed scaled parameters presented by Yakirevich et al [1].

RESULTS AND DISCUSSION

The vibration identification method was applied at the cases of table 1. The results are plotted in figure 5. The figure presents time-series that are measured separately for each case, and not simultaneous measurements. The cases of the same cutoff orientation are plotted together for comparison. It is visible that the intensity fluctuation has been decreased in the cases of increased rigidity. General decrease of amplitude after the rigidity increase indicates that the source of vibration is indeed the deformation of components. The most dramatic amplitude decrease appears in the vertical cutoff case. Case H2 intensity fluctuations are steadier than case H1 with a more distinct sinewave behavior.

Table 2. Intensity fluctuation and density gradient deviation results

Case	Max Intensity fluctuation [%]	Intensity RMSe	Max $\partial\rho/\partial y$ deviation [%]	Mean $\partial\rho/\partial y$ deviation [%]
H1	21.4	7.11	18.34	4.1
V1	17.2	3.89	15.81	1.95
H2	13.5	4.99	8.95	2.16
V2	2.8	0.74	1.8	0.31

Table 2 summarizes the maximum fluctuation of intensity and overall level of deviation based on

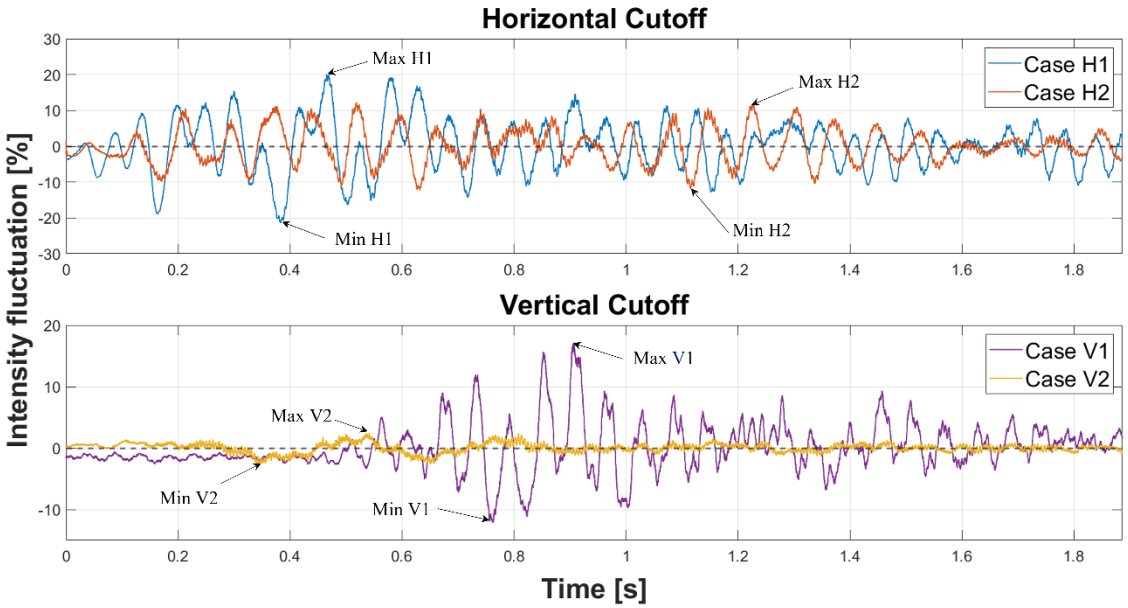

Figure 5. Intensity fluctuation results

Root Square Mean error (RMSe). After the rigidity increase the maximum fluctuation has dropped by 7.9% for the horizontal cutoff test and 10.7% for the vertical. Furthermore, the RMSe level also decreased more significantly in the vertical orientation. It was decreased by 3.22 at the less affected horizontal orientation case and 4.25 at the vertical orientation. In addition, in the cases of increased rigidity the vibrations are damped faster. This contributes to the decrease of the overall level of fluctuation. It is implied that the system is mostly deformed by higher-level forces of the supersonic flow rather than the excitation of lower-level forces in the acceleration and deceleration phases.

Matching of characteristic overall intensity with the fluctuation peaks validates the correctness of the identification method. In figure 6, the images corresponding to the start of recording (as reference), minimum intensity, mean intensity and maximum intensity, are presented. The minimum and maximum intensity images of each case match the noted peaks on the plot of Figure 5 for the respective cases. Similar flow structure in all cases indicate that the forces applied on the vanes are in the same order of magnitude and similarly applied.

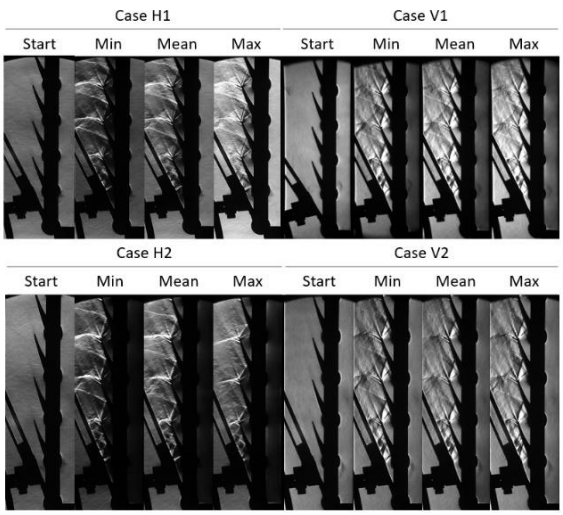

Figure 6. Schlieren picture with fluctuating overall intensity corresponding to indicated instants in figure 4

In case V2 the deviation of intensity is minimum and cannot be easily detected with the naked eye. Although the fluctuation was very small, it was resolved through the vibration quantification method. The method proposed in this document can be useful as an assessment tool for theoretically vibration free systems. After the acquisition of the intensity fluctuation the calculation of the density gradient deviation can be calculated through the proposed procedure.

The deviation in density gradient is calculated from equation 7 based on the new CO% and the respective overall intensity of each frame. Since the intensity fluctuates around the mean intensity the deviation does not reach the highly non-linear parts of the fitted surface. Thus, the conversion of intensity fluctuation to density gradient change is almost linear.

The density gradient vibrating deviation results are presented in Figure 7. The density gradient has the same trend as the intensity fluctuation but in opposing manner. This was expected since the bright side of the calibration lens is considered to refract the light in negative refraction angle. The measuring range of the current schlieren system is found to extend from -0.2 to 0.2 $kg/(m^3 \times mm)$ (also visible at the map of figure 2c). Thus, the maximum gradient that can be resolved is 0.4 $kg/(m^3 \times mm)$. Based on that, the percentages of density gradient deviation due to vibrations are noted in table 2. The maximum deviation for

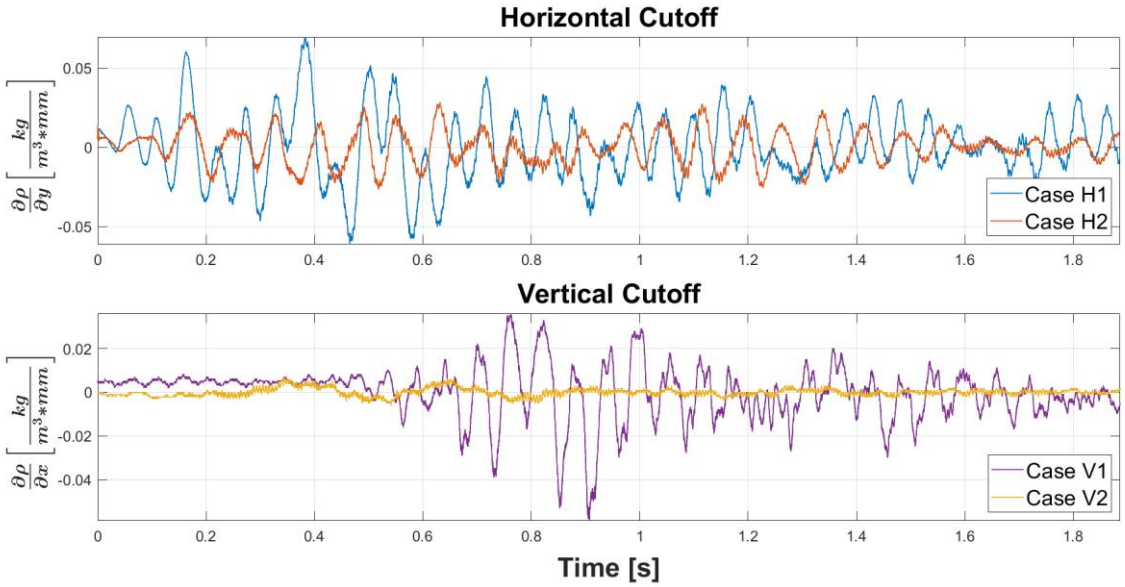

Figure 7. Density gradient deviation

horizontal and vertical cutoff has decreased by 9.39% and 14.01% respectively. The maximum deviation follows the pattern of intensity fluctuation for all cases. The deviation is lower for the density gradients than the intensity fluctuation for all cases. This happens because the intensity change is based on the dynamic range of the camera (10-bit, 1024 DL) but the density gradient deviation is based on the measuring range. The measuring range increases asymptotically near the limits of the dynamic range in a non-linear manner. This nonlinear behavior away from the curve's center "stretches" the range of resolved density gradients in comparison to the linear dynamic range of the camera. As a result, the two deviations do not match when expressed in percentages.

The mean error cannot be acquired by averaging the deviated density gradient since it fluctuates around a mean value. The mean error can be assumed to have sinewave behavior that follows the trend of the higher amplitude vibration in the dominant frequency. In order to acquire this sinewave a Fast Fourier Transformation (FFT) is conducted for each case. The results of FFT are presented in Figure 8. The mean error for horizontal and vertical cutoff was decreased by 1.94% and 3.79% respectively after the increase of rigidity. One can isolate a steady part of the vibration for each case in order to get a quasi-steady frequency. The ability of the method to predict unsteady vibrating behavior was one of the goals of this study and therefore the FFT was applied to the vibrations of the whole flow cycle. A frequency of 170 Hz with low amplitude appeared for all the cases.

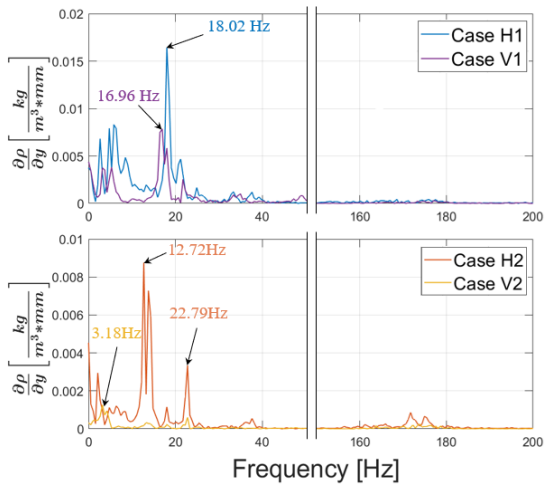

Figure 8. Fast Fourier Transformation

The vibration of the individual optical components (not the aluminum breadboard) is believed to create higher frequency vibrating movement of the knife's edge. These frequencies can be considered negligible due to the significantly lower amplitude in comparison to the dominant frequency amplitude. However, being able to resolve low amplitude vibrations with high frequency makes the method applicable to more robust systems in which the amplitude of vibrations is smaller. The resolved amplitude of the vibrations is confined to the dimensions of the focal point (after saturation vibrations cannot be resolved) and the highest frequency from the frame rate of the camera. One can vary the radius/diameter of the light beam at the knife's edge position depending under investigation amplitude of the vibrations.

CONCLUSIONS

The vibration identification method was applied in 4 cases of experiments with vibrating behavior. Two knife's edge orientations were tested, and the flexural rigidity of the system was increased from 6.05 to 291.7 $Pa \times m^4$ in order to evaluate the method's performance in lower relative knife's edge movement. After the flexural rigidity was increased from, the maximum overall fluctuation of

intensity was decreased resulting in 9.39% and 14.01% density gradient deviation reduction for horizontal and vertical cutoff respectively.

The source of relative vibrations was identified to be the deformation vibrations of the schlieren supporting system. Positive and negative peaks of vibrations matched the intensity of the respective images. Case V2 initially thought to be free of vibrations, but application of the method resolved a vibrating behavior impossible to detect with the naked eye. In the increased rigidity cases, FFT analysis showed decrease in the dominant frequencies and appearance of secondary frequencies with lower amplitude A behavior of significantly low amplitude vibration was observed for all cases, at the frequency of 170 Hz. The methods successfully resolved all vibration frequencies including the lower amplitudes.

Applying the method in schlieren measurements of more rigid systems can identify fine vibrations that would be very difficult to identify otherwise. The advantage of the proposed vibration quantification method is that it is only based on principle of calibrated schlieren, and any external instrumentation is unnecessary.

ACKNOWLEDGMENTS

The authors acknowledge the financial support of Minerva Research Center (Max Planck Society Contract No. AZ5746940764).

REFERENCES

[1] E. Yakirevich, R. Miezner, B. Leizeronok, and B. Cukurel, “Continuous Closed-Loop Transonic Linear Cascade for Aerothermal Performance Studies in Microturbomachinery,” *J. Eng. Gas Turbines Power*, vol. 140, Jan. 2018,

[2] J. A. Dunsby, “Schlieren Tests on some Conventional Cascades,” p. 16.

[3] Z. Zhou, H. Liu, K. Zhou, and C. Li, “Shock System Model of Highly Loaded Turbine Cascade,” *J. Aerosp. Eng.*, vol. 33, no. 1, p. 04019107, Jan. 2020.

[4] S. Loose, H. Richard, T. Dewhirst, and M. Raffel, “Background oriented schlieren (BOS) and particle image velocimetry (PIV) applied for transonic turbine blade investigations,” p. 8.

[5] T. Léonard, L. Y. M. Gicquel, N. Gourdain, and F. Duchaine, “Steady/Unsteady Reynolds-Averaged Navier–Stokes and Large Eddy Simulations of a Turbine Blade at High Subsonic Outlet Mach Number,” *J. Turbomach.*, vol. 137, no. 4, p. 041001, Apr. 2015.

[6] M. Passmann, S. aus der Wiesche, and F. Joos, “Focusing Schlieren Visualization of Transonic Turbine Tip-Leakage Flows,” *Int. J. Turbomach. Propuls. Power*, vol. 5, no. 1, p. 1, Jan. 2020.

[7] M. J. Hargather and G. S. Settles, “A comparison of three quantitative schlieren techniques,” *Opt. Lasers Eng.*, vol. 50, no. 1, pp. 8–17, Jan. 2012.

[8] L. Venkatakrishnan and G. E. A. Meier, “Density measurements using the Background Oriented Schlieren technique,” *Exp. Fluids*, vol. 37, no. 2, pp. 237–247, Aug. 2004.

[9] A. J. Harris, P. A. Kreth, C. S. Combs, and J. D. Schmisseur, “Laser Differential Interferometry and Schlieren as an Approach to Characterizing Freestream Disturbance Levels,” presented at the 2018 AIAA Aerospace Sciences Meeting, Kissimmee, Florida, Jan. 2018.

[10] C. B. Wells, “Knife-Edge Controller for a Schlieren System,” *Appl. Opt.*, vol. 4, no. 7, p. 815, Jul. 1965.

[11] C. Alvarez-Herrera, D. Moreno-Hernández, B. Barrientos-García, and J. A. Guerrero-Viramontes, “Temperature measurement of air convection using a Schlieren system,” *Opt. Laser Technol.*, vol. 41, no. 3, pp. 233–240, Apr. 2009.

[12] “Researches on the Refraction, Dispersion, and Sensitiveness of Liquids,” p. 28, 2022.

[13] G. S. Settles, *Schlieren and Shadowgraph Techniques*. Berlin, Heidelberg: Springer Berlin Heidelberg, 2001.

[14] V. K. I. for F. Dynamics, *Measurement Techniques in Fluid Dynamics : an Introduction*. Von Karman Institute for Fluid Dynamics, 2001. [Online]. Available:

[15] S. Kook, M. K. Le, S. Padala, and E. R. Hawkes, “Z-type Schlieren Setup and its Application to High-Speed Imaging of Gasoline Sprays,” Aug. 2011.

[16] Y. Kojima, C.-A. Yeh, K. Taira, and M. Kameda, “Resolvent analysis on the origin of two-dimensional transonic buffet,” *J. Fluid Mech.*, vol. 885, p. R1, Feb. 2020.

[17] M. Tsinoglou, “Micro gas turbine blade Flow characteristics evaluation and acoustic flow control for pressure recovery using quantitative schlieren imaging,” p. 47.

[18] T. P. Davies, “Schlieren photography—short bibliography and review,” *Opt. Laser Technol.*, vol. 13, no. 1, pp. 37–42, Feb. 1981.

[19] A. Pavlov, A. Pavlov, and M. Golubev, “Some aspects of a Schlieren technique sensitivity increasing,” p. 1.

[20] L. D. Hylton, M. S. Mihelc, E. R. Turner, D. A. Nealy, and R. E. York, “Analytical and experimental evaluation of the heat transfer distribution over the surfaces of turbine vanes,” May 1983.